Supporting information for

Encapsulated Ruthenium sites in reaction microenvironment-regulated UiO-66 for stable acetylene hydrochlorination

Digao Chai[a], Qidi Liu[a], Yunsheng Dai[b], Yongsheng Xu[a]*, Yu Zi[a], Shuo Yang[a], Yanzhao Dong[a], Dongyang Xie[a], Jinli Zhang[a, c], Haiyang Zhang [a]*

[a] School of Chemistry and Chemical Engineering/State Key Laboratory Incubation Base for Green Processing of Chemical Engineering, Shihezi University, Shihezi 832000, P. R. China

[b] Yunnan Precious Metals Lab Co., Ltd, Kunming 650106, P. R. China

[c] School of Chemical Engineering and Technology, Tianjin University, Tianjin 300354, P. R. China

* Corresponding author:

Yongsheng Xu

E-mail: 2016207134@tju.edu.cn

Haiyang Zhang

E-mail: zhy198722@163.com

Tel.: +86-993-2057006; Fax: +86-993-2057210.

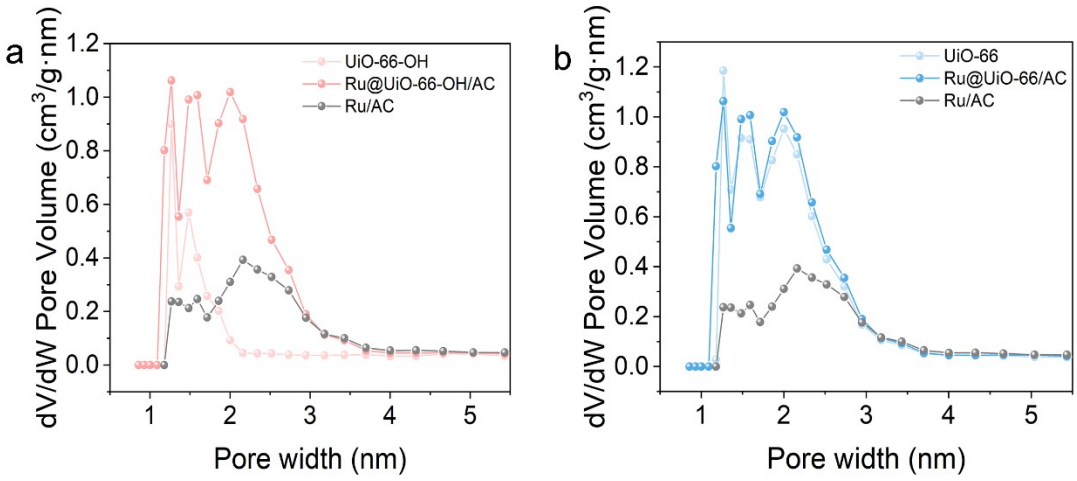

Fig. S1. Pore size distribution image of (a) Ru@UiO-66-OH/AC and (b) Ru@UiO66/AC.

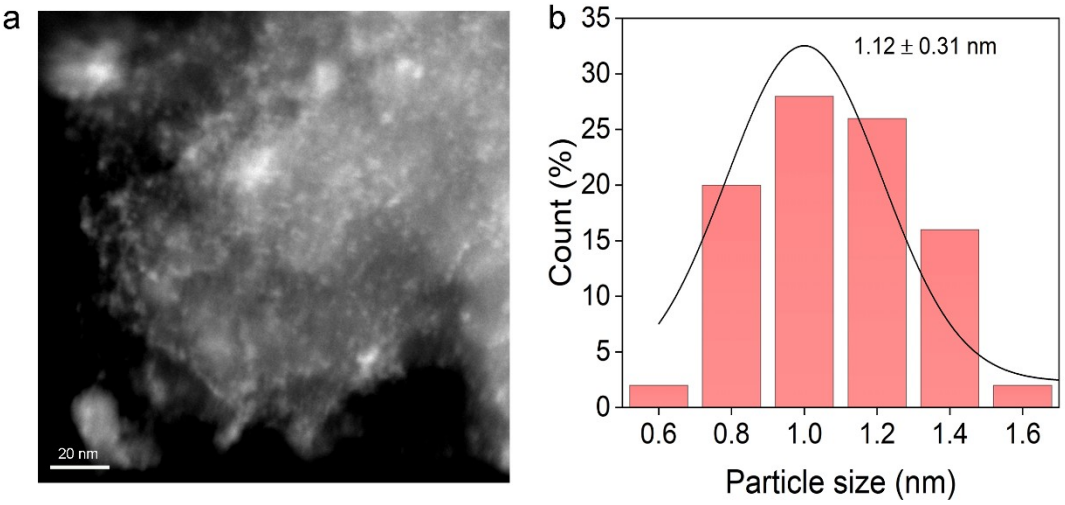

Fig. S2. (a) HADDF-TEM image of fresh Ru/AC and (b) particle size distribution images.

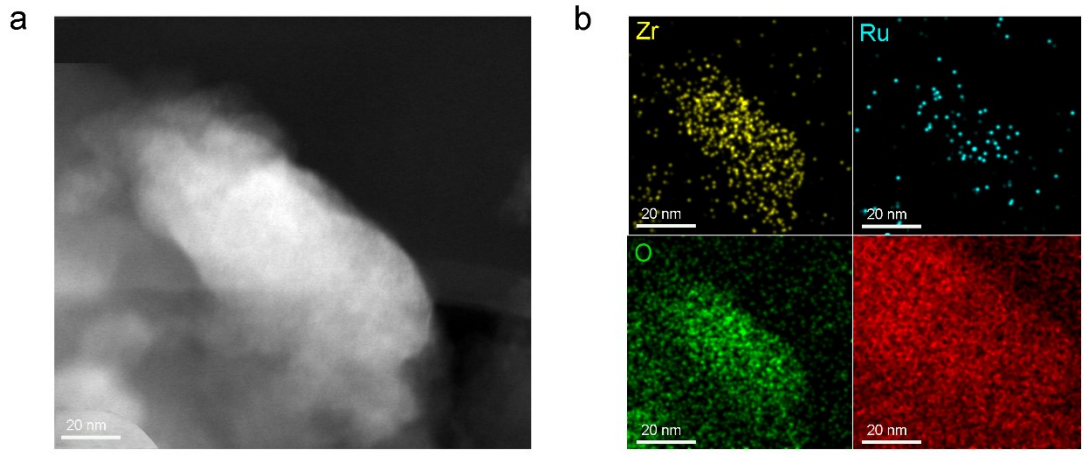

Figure S3. (a) HADDF-TEM image and (b) the relative elemental mapping images of fresh Ru@UiO-66/AC catalyst.

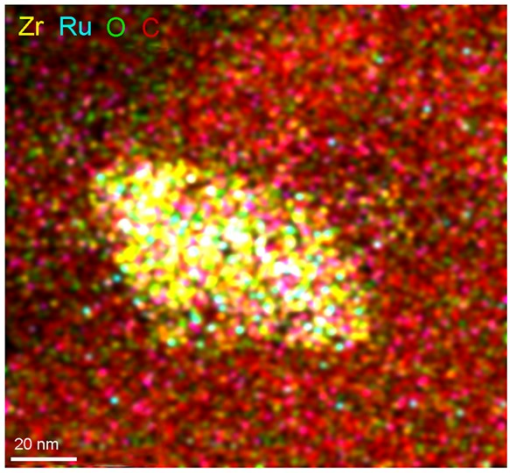

Fig. S4. Overlay image of Ru, O, C and Zr elements.

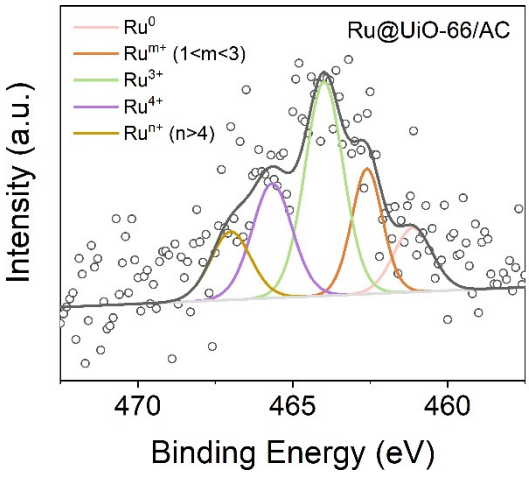

Fig. S5. Ru *3p* XPS spectrum of Ru@UiO-66/AC.

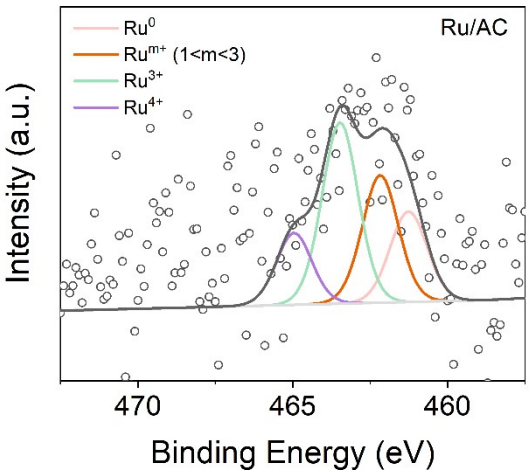

Fig. S6. Ru *3p* XPS spectrum of Ru/AC.

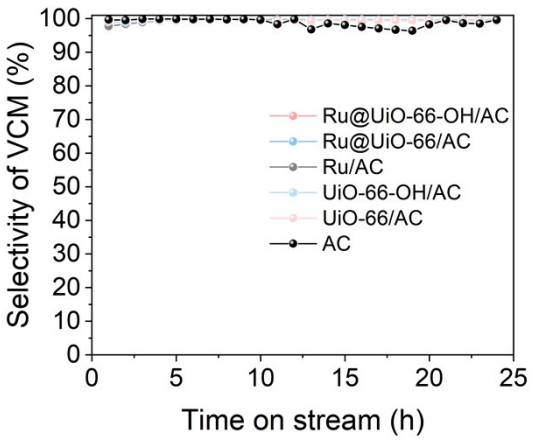

Fig. S7. Selectivity to VCM of Ru-based catalysts and UiO-66-based catalysts.

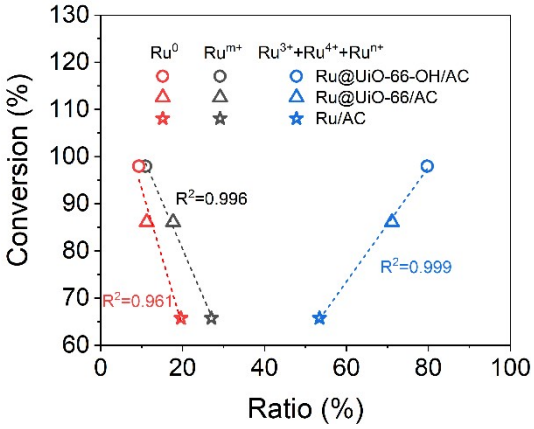

Fig. S8. Relationship between chemical state of Ru species and conversion.

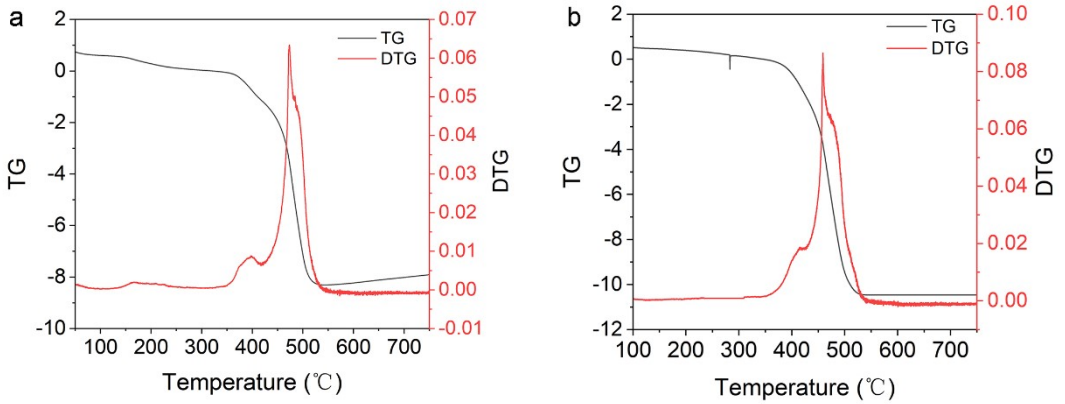

Figure S9. TGA and DTG curves of the fresh (a) Ru@UiO-66-OH/AC and (b) Ru@UiO-66/AC.

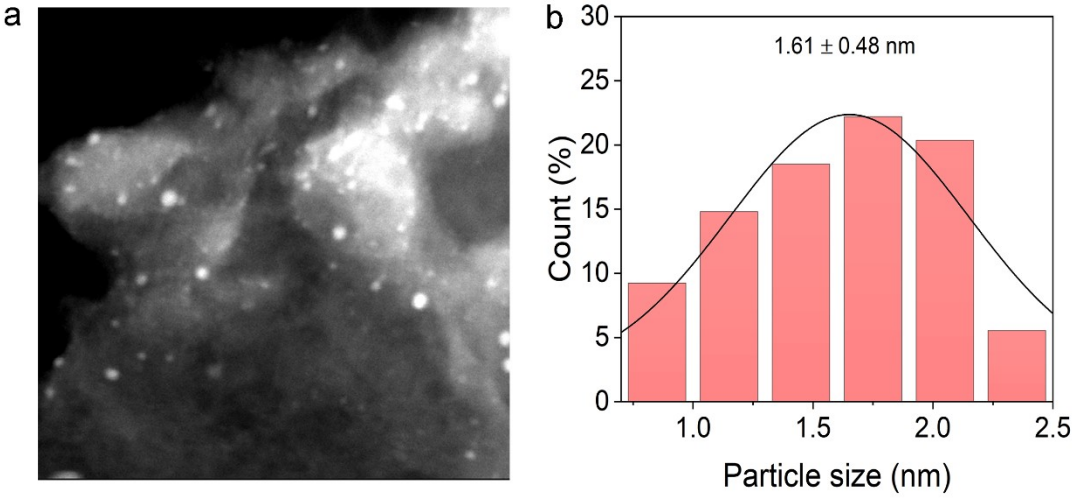

Figure S10. (a) HADDF-TEM image and (b) particle size distribution of used Ru/AC.

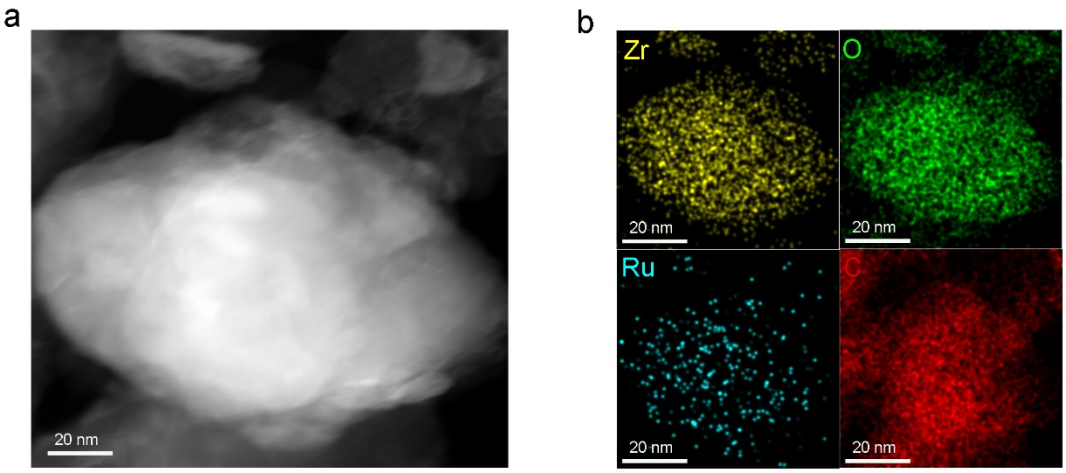

Figure S11. (a) HADDF-TEM image and (b) the relative elemental mapping images of used Ru@UiO-66/AC catalyst.

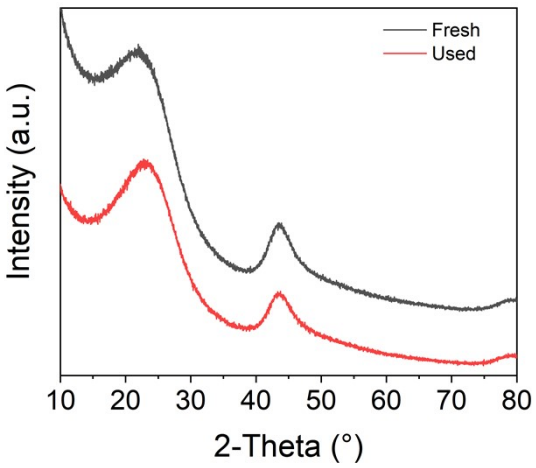

Figure S12. XRD patterns of baseline catalyst.

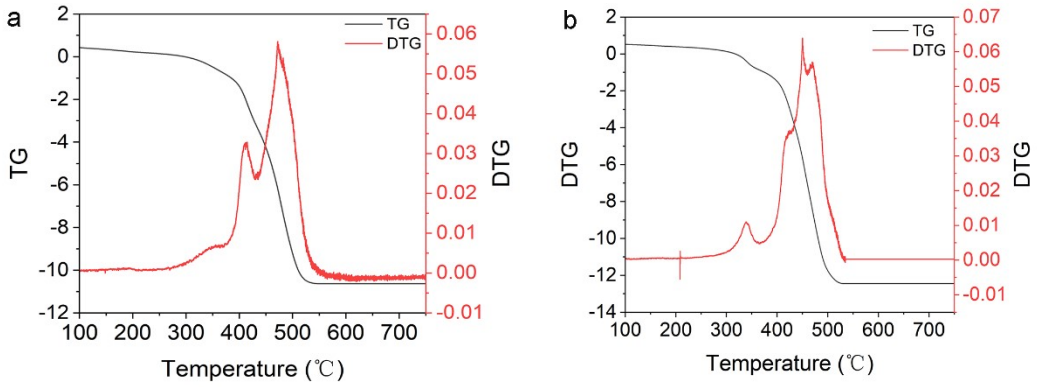

Figure S13. TGA and DTG curves of the used (a) Ru@UiO-66-OH/AC catalyst and (b) Ru@UiO-66/AC catalyst.

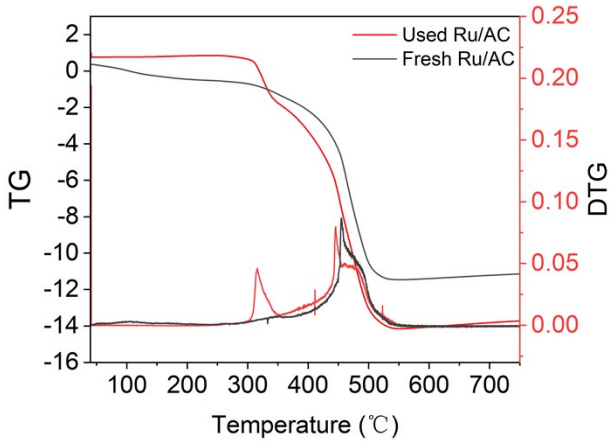

Figure S14. TGA and DTG curves of the fresh and used Ru /AC catalyst.

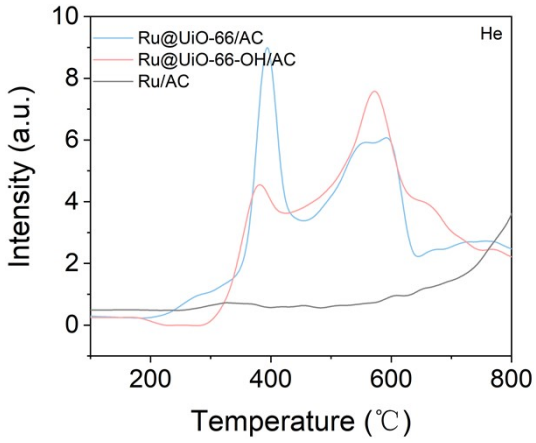

Figure S15. He-TPD profiles of the Ru@UiO-66-OH/AC, Ru@UiO-66/AC and Ru/AC.

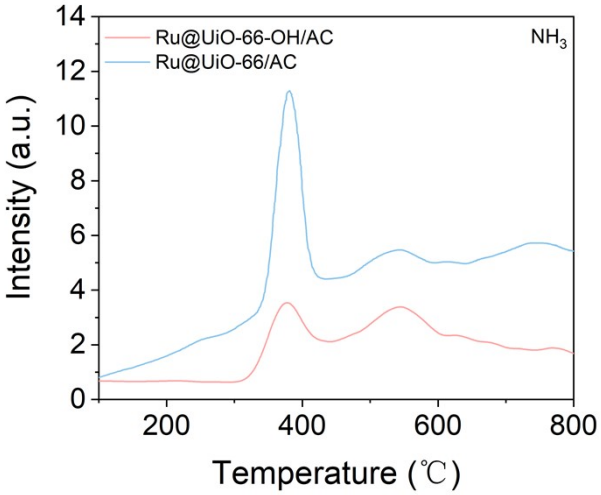

Figure S16. NH_3-TPD profiles of the Ru@UiO-66-OH/AC, Ru@UiO-66/AC and Ru/AC.

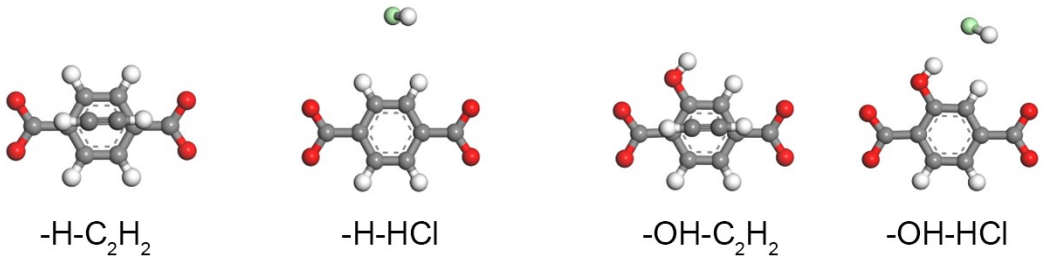

Figure S17. Adsorption models of C_2H_2 and HCl on the unit of linkers. Atom: C, grey; H, white; O, red; Cl, green.

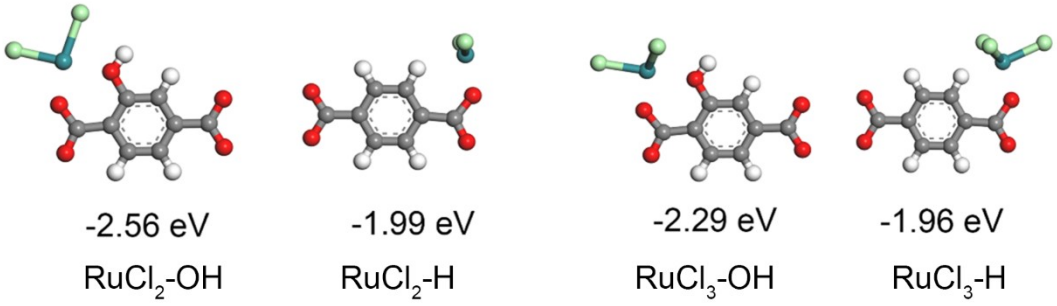

Figure S18. Formation models and energies between $RuCl_x$ species and the relative linkers. Atom: C, grey; H, white; O, red; Cl, green.

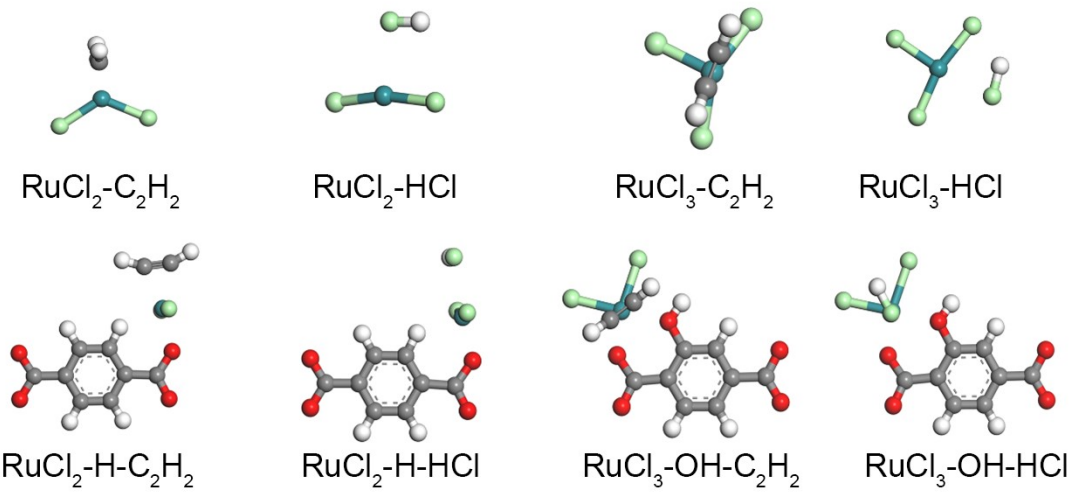

Figure S19. Adsorption models of C_2H_2 and HCl on the relative Ru sites. Atom: C, grey; H, white; O, red; Cl, green.

Table S1. The relative content of Ru species in Ru@UiO-66-OH/AC and Ru@UiO-66/AC catalysts.

Catalyst		Ru@UiO-66-OH/AC	Ru@UiO-66/AC	Ru/AC
Ru^{0+}	Binding energy (eV)	460.98	461.12	461.26
	Ratio (%)	9.33	11.23	19.58
Ru^{m+} (1<m<3)	Binding energy (eV)	462.52	462.6	462.17
	Ratio (%)	10.95	17.68	27.01
Ru^{3+}	Binding energy (eV)	463.77	463.99	463.47
	Ratio (%)	36.73	37.50	38.41
Ru^{4+}	Binding energy (eV)	465.48	465.67	464.96
	Ratio (%)	33.05	21.08	14.99
Ru^{n+} (n>4)	Binding energy (eV)	467.26	467.01	/
	Ratio (%)	9.94	12.51	/